J Mater Sci (2009) 44:4911–4918
DOI 10.1007/s10853-009-3750-y

Weibull modulus of nano-hardness and elastic modulus of hydroxyapatite coating

Arjun Dey · Anoop K. Mukhopadhyay · S. Gangadharan · Mithilesh K. Sinha · Debabrata Basu

Received: 1 April 2009 / Accepted: 15 July 2009 / Published online: 29 July 2009

Abstract Here we report the microstructural dependence of nano-hardness (H) and elastic modulus (E) of microplasma sprayed (MIPS) 230 μm thick highly porous, heterogeneous hydroxyapatite (HAP) coating on SS316L. The nano-hardness and Young's modulus data were measured on polished plan section (PS) of the coating by the nano-indentation technique with a Berkovich indenter. The characteristic values of nano-hardness and Young's modulus were calculated through the application of Weibull statistics. Both nano-hardness and the Young's modulus data showed an apparent indentation size effect. In addition, there was an increasing trend of Weibull moduli values for both the nano-hardness and the Young's modulus data of the MIPS-HAP coating as the indentation load was enhanced from 10 to 1,000 mN. An attempt was made in the present work, to provide a qualitative model that can explain such behavior.

Introduction

Compared to the conventional macroplasma (MAPS) sprayed coatings, the microplasma sprayed (MIPS) hydroxyapatite (HAP) coatings are recently gaining more popularity as a bioactive ceramic coating for prosthetic implant applications. However, such applications require characterization and understanding of several important mechanical properties, e.g., nano-hardness (H) and Young's modulus (E) at local microstructural level [1–16]. Recently, the present author and co-workers reported bonding strength of 13 MPa, fracture toughness of about 0.6 MPa $m^{0.5}$, nano-hardness of 5–1.5 GPa, and Young's modulus of 100–60 GPa at 170–3,000 nm depth of MIPS-HAP coatings on SS316L substrate [1–4]. Researchers have reported the nano-hardness [1–4, 7–11, 13–16] and Young's modulus [2–14, 16] values of the HAP [1–13, 16] and HAP composite [9, 14] coatings deposited by plasma spraying [1–6], laser-assisted process [8–10, 12, 16], sol–gel process [14, 15], sputtering [10, 11], and other thermal spraying techniques [9, 13, 15]. The measurements were taken by nanoindentation [1–16] technique with a Berkovich [1–7, 9–11, 13–15], Vicker's [8], and spherical indenter [16]. However, systematic study of both the hardness and elastic modulus measured by the nanoindentation technique under a variety of applied loads on HAP coating are rare [2, 3]. It was also found in general that the scatter in data was very high for the plasma sprayed coatings, presumably due to the highly heterogeneous and porous structure of the coatings [2, 17–19].

So, the major objective of the present study was to characterize the nano-hardness and elastic modulus on the plan section of MIPS-HAP coatings measured by the nanoindentation technique with Berkovich indenter under a variety of loads in the range of 10–1,000 mN loads. In addition, the Weibull statistical analysis has been utilized here to obtain the characteristic values of nano-hardness and Young's modulus for useful exploitation in terms of structural designing purpose. Further, an attempt was made in the present work for the first time, to provide a qualitative model that can explain the increasing trend of Weibull moduli data with load.

A. Dey · S. Gangadharan · M. K. Sinha · D. Basu
Bio-Ceramics and Coating Division, Central Glass and Ceramic Research Institute, Kolkata 700032, India

A. Dey · A. K. Mukhopadhyay (✉)
Mechanical Test Section, Analytical Facility Division, Central Glass and Ceramic Research Institute, 196, Raja S.C. Mullick Road, Kolkata 700032, India
e-mail: anoopmukherjee@cgcri.res.in

Materials and methods

Atmospheric microplasma spraying (MIPS) of sintered granules of HAP (d_{50}-67 μm, Ca/P-1.67 [1, 2]) powder was carried over SS316L substrates (15 × 15 × 2 mm^3). Prior to microplasma spraying, substrates were grit blasted with alumina grits to R_a ~2.5 μm. The MIPS process was carried out utilizing very low (~1.5 kW) plasmatron power (Miller Maxstar 200 SD 2.5 kW) with argon as both primary and secondary gas. The coated samples were post-heat-treated at 600 °C in air. The microstructural characterizations and coating thickness measurements were carried out using scanning electron microscopy, SEM (s430i, Leo, UK), field emission scanning electron microscopy, FE-SEM (Supra VP35 Carl Zeiss, Germany), and an image analyzer (Leica Q500MC, UK). Prior to insertion in the sample chamber for electron microscopy, a 50–70 nm carbon/gold coating was deposited on the HAP coating by the arc deposition technique to avoid charging.

Nanoindentations were carried out using a commercial machine (Fischerscope H100-XYp; Fischer, Switzerland) equipped with a Berkovich tip. The depth and force sensing resolutions of the machine were 1 nm and 0.2 μN, respectively. The machine was calibrated following DIN 50359-1 standard with nanoindentation-based independent evaluation of hardness, H (about 4.14 GPa) and Young's modulus, E (about 84.6 GPa) values of a reference glass block (BK7, Schott, Germany). The calibration was repeated before each and every experiment. The reason for this exercise was twofold. The first was to ensure that the calibration values of hardness and Young's modulus for the reference glass block, Schott BK-7, a standard material was within the prescribed limits of experimental error. The second was to ensure that the load–depth plot was free from any temporal effects such as thermal drifts etc. This procedure of calibration check was deliberately done also to check the extent of reproducibility of the experimental data, which was found to be satisfactory.

The present experiments were conducted at nine different loads in the range of 10–1,000 mN on the plan section of the polished coatings. The Berkovich indenter had a tip radius of about 150 nm and a semi-apex angle of 65.03°. Both the loading and unloading time were kept at 30 s. The data on H and E were evaluated, as mentioned earlier, according to DIN 50359-1 standard from the load versus depth of penetration plots using the well-established Oliver and Pharr (O–P) method [20]. At least 25 indents were made at each test load on the coating. Thus, altogether at least 125 data from nanoindentation experiments were analyzed to evaluate the E and H values. The high, characteristic scatter in data for E and H values of the highly porous, heterogeneous coating was treated with the well-established Weibull distribution. This particular statistical method has been widely utilized to calculate the characteristics values for various mechanical properties of heterogeneous materials; for example to calculate the micro-hardness and Young's modulus of thermal barrier coatings on Ti-alloys [17–19], MIPS-HAP coatings on SS316L [2], etc. For this purpose, the two-parameter Weibull distribution function was employed. The Weibull distribution function provides the probability, p, for a given parameter, x, as [2, 17–19]:

$$p = 1 - \exp\left[-(x/x_o)^m\right] \quad (1)$$

where x_o is known as the scale parameter where the probability of occurrence is 63.2% and "m" is the Weibull modulus. The value of "m" is a dimensionless quantity and indicates the measure of scatter in the data. The magnitude of "m" increases with decreasing scatter. The survival probability of the ith observation in the data arranged in ascending order can be expressed as [2, 17–19]:

$$p = (i - 0.5)/N \quad (2)$$

where N is the total number of observations. Taking ln for two times of both the sides and simplifying, Eq. 1 can be expressed as:

$$\ln[\ln\{1/(1-p)\}] = m[\ln(x) - \ln(x_o)] \quad (3)$$

The values of m and x_o are obtained by fitting the experimental data to Eq. 3, by least square regression. The slope of the straight line will give the value of Weibull modulus (m) and the intercept on the "Y" axis will give the value of scale parameter (x_o). Finally, by setting the value of ln [ln $\{1/(1 - p)\}$] equal to zero and placing the values of m and scale-parameter in Eq. 3, one can easily calculate the characteristic value (x_o) of the related parameter, x. The characteristic values (x) are of great engineering importance as it provides the designer with a unique and dependable value of the required parameter. In the present study, x was hardness and Young's modulus. The corresponding characteristic values were termed as H_{char} and E_{char}.

Results and discussions

The FE-SEM photomicrographs of both plan section and cross section of the MIPS-HAP coating on SS316L substrates are shown in Fig. 1a, b. The spatial density of pores, cracks, and defects were very high on the plan section, Fig. 1a. The coating had a thickness of about 230 μm (Fig. 1b). These features are schematically illustrated in Fig. 2.

As mentioned above, the coating presents a high level of porosity and heterogeneity. Due to this microstructural peculiarity, the mechanical characterization of such a

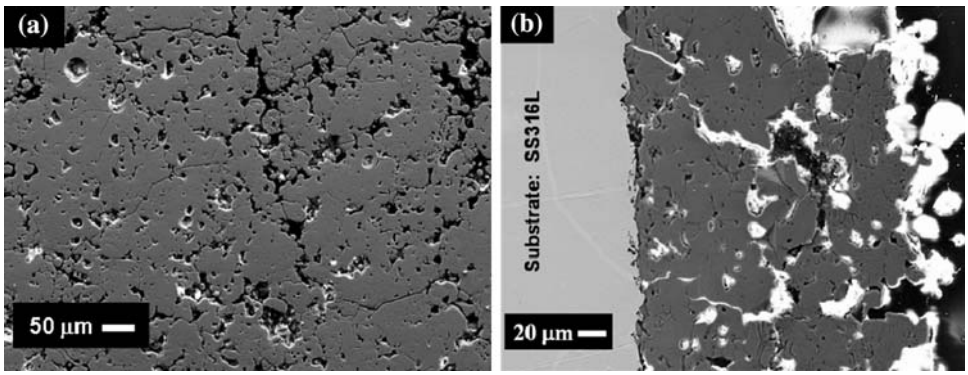

Fig. 1 FE-SEM photomicrographs of the polished coating **a** plan and **b** cross section

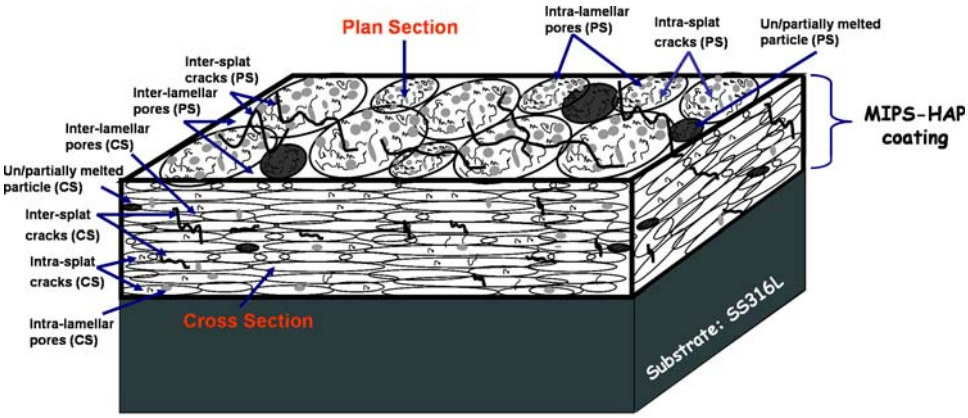

Fig. 2 Schematic of the structure and nature of the MIPS-HAP coating

coating is obviously rendered very difficult. That is why it was decided to employ a Weibull approach so that characteristic values of both nano-hardness and Young's modulus can be obtained to analyze the influence of indentation load, if any, on the data. Accordingly, at first the Weibull distribution fittings for the nano-hardness data of the coating are displayed for the low (10–100 mN) loads in Fig. 3a and for the high (300–1,000 mN) loads in Fig. 3b. Similarly, the Weibull distribution fittings for the Young's modulus of the coating, as determined by the nanoindentation experiment are displayed for the low (10–100 mN) loads in Fig. 4a and for the high (300–1,000 mN) loads in Fig. 4b.

Next, the characteristic values of nano-hardness and Young's modulus were calculated from this data through the application of Weibull statistics, following refs. [2, 17–19] as mentioned earlier. On the plan section the characteristic nano-hardness and Young's modulus showed values in the range of about 5–1.5 GPa (Fig. 5a) and 100–63 GPa (Fig. 5b), respectively, as the nanoindentation load was varied in the range of 10–1,000 mN. The hardness data apparently suggest the presence of a strong indentation size effect (ISE), i.e., load dependence of the data. Nevertheless, ISE is a much more complex problem than what is reflected in a simplistic fashion in the data and that is why it is preferable to term it as an "apparent ISE".

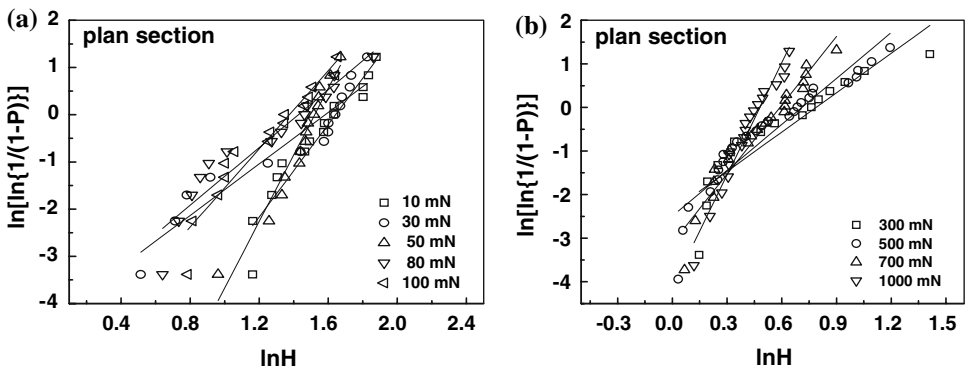

Fig. 3 Weibull plots of hardness data of MIPS-HAP coating at **a** 10–100 mN and **b** 300–1,000 mN for the plan section

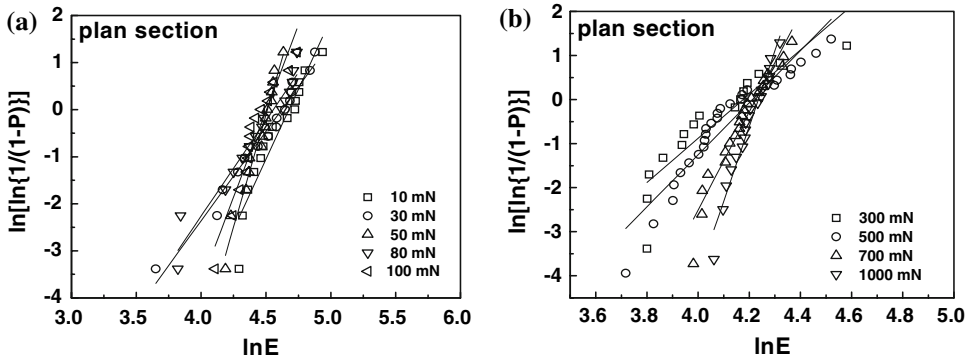

Fig. 4 Weibull plots of Young's modulus data of MIPS-HAP coating at **a** 10–100 mN and **b** 300–1,000 mN for the plan section

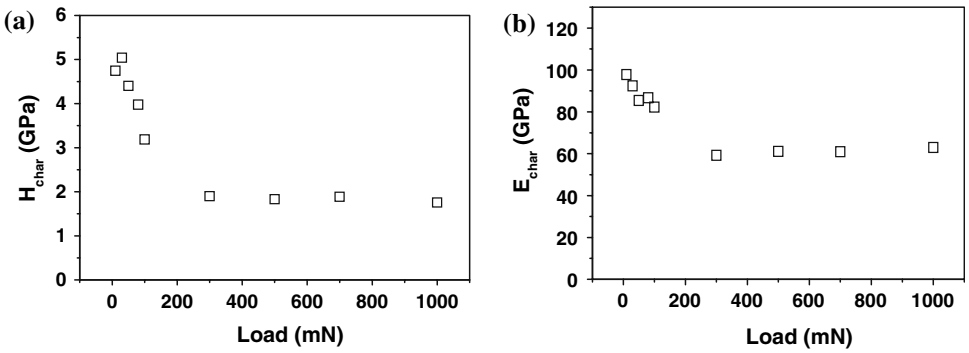

Fig. 5 **a** Nano-hardness and **b** Young's modulus on plan section of MIPS-HAP coating

Indentation size effect (ISE) as encountered in both metallic [21] and brittle [22] materials as well as nano-crystalline and quasi-crystalline materials [23, 24], is a significant phenomenon in micro- and nanoindentation tests describing the increase in hardness values with decrease of the indentation loads. In the past few decades, a number of explanations have been developed for ISE. These include: energy balance concept [25], the well-established strain gradient plasticity theory [26], and dislocation nucleation [27]. In addition, efforts were made to explain ISE in terms of various other factors. These involve among others notably, the variation of contact surface [28], friction between the surface and the indenter [29], micro-fracture processes [30], presence of residual surface stress [31], existence of dissipation energy associated with the contact surfaces [32], influence of the substrate for thin nanometric coatings [33], etc. Furthermore, researchers tried to explain the origin of ISE in terms of various other concepts. These incorporate among others notably the concept of the minimum resistance on the surface [34], proportional specimen resistance (PSR) concept [35], modified PSR concept [36], etc. Researchers also opined spatial gradient in flaw density [18] might contribute to ISE in ceramic thermal barrier coatings. The present author and co-workers suggested that reduction in solid load bearing contact area inside the indentation volume [2] may result in ISE observed in plasma sprayed ceramic coating. Clearly, the genesis of ISE in solids and in particular, in ceramic coatings is yet to be unequivocally established and thereby pose an interesting challenge for the researchers.

However, the most critically appraised and theoretically well-founded explanation of ISE is believed to be due to the organization and re-organization of the dislocation network under the indent during the indentation process. The model that describes this phenomenon adequately is that of Nix and Gao [26]. The model is based on the dislocation theory of Taylor [37, 38]. This model has been successfully applied on dense, massive crystals without heterogeneity, e.g., defect in the structure and successfully predicts the increase of hardness when the indentation depth decreases. The parameters of the model are connected to the dislocation density and a scale-factor in depth in the following fashion [26]:

$$\left(\frac{H}{H_0}\right)^2 = 1 + \frac{h^*}{h} \tag{4}$$

where H was the experimentally measured nano-hardness at a depth h, h^* was a characteristic length that depends on the properties of indented material and the indenter angle, and H_0 was the indentation hardness at infinite depth. Accordingly, it was decided to fit the whole data of present work to Eq. 4.

The result of this exercise is shown in Fig. 6. Clearly, the model could rightly predict the basic trend of increase in nano-hardness with decrease in depth as observed in the experimental data. This observation also highlights the

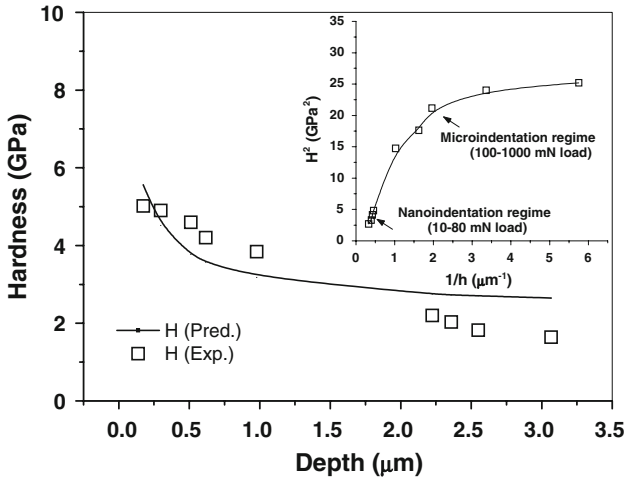

Fig. 6 Experimental and predicted hardness as a function of depth and (*inset*) square of indentation hardness, H^2 as a function of reciprocal depth, $1/h$

primary success of the Nix and Gao model. The fitting of present data to Nix and Gao model [26] predicts $H_0 = 2.37$ GPa and $h^* = 0.79$ μm. The predicted value of H_0, however, was very much lower than that of dense bulk HAP, e.g., 6 GPa [39].

Although the predictions appear reasonable, a critical look at the experimental data itself indicates that indeed there were two slopes (e.g., nanoindentation and micro-indentation regime) present in the plot of square of indentation hardness, H^2, as a function of reciprocal depth, $1/h$, (Fig. 6, inset). The slope for nano-hardness data up to a depth of about 0.75 μm was clearly different from that of nano-hardness data obtained at depth ≥1 μm. This was not really surprising. It may be mentioned here that while studying the hardness of MgO, Huang et al. [40] also found two straight lines to represent the model of Nix and Gao in the two "scales of measurement", the nanoindentation data at lower depth and the micro-indentation data at higher depth [see, e.g., Fig. 6 of ref. 40].

It was also interesting to note that in our experimental data on HAP coating, the loads corresponding to about 0.15–0.75 μm of depth were about 10–80 mN, which indeed pertains more to a characteristic nanoindentation load regime. However, the other higher load range, e.g., those corresponding to depth of about 1–3 μm were about 0.1–1 N, which indeed reflects more of a characteristic micro-indentation load regime, especially near the higher end of the load range utilized. Therefore, it was not totally unexpected to have two different slopes existing in the nano-hardness versus depth plot of present work, Fig. 6.

It was noted further that when the nano-hardness data corresponding to loads of about 10–80 mN was analyzed using the Nix and Gao model, it predicts $H_0 = 4.13$ GPa and the characteristic length scale $h^* = 91$ nm. The predicted value of H_0 compared favorably with that of dense bulk HAP, e.g., 6 GPa [39], albeit a little on the lower side, as expected presumably due to porosity. This information also provides further support to the notion that at least a part of the data reflects an ISE explainable in terms of the classical strain gradient plasticity concept.

In addition, it was very interesting to note that for MgO ceramic also, the characteristic length scale was estimated as $h^* \sim 96$ nm [40]. The comparison of the data from present work and that from Hunag et al. [40] would seem to suggest that the characteristic length scale along depth up to which the gradient in local strain would affect the nano-hardness data the maximum would be about 100 nm for typical ceramics like MgO and plasma sprayed ceramic coatings like the present HAP coating. It would be obviously meaningless to separately apply Nix and Gao model to depths higher than 100 nm and hence, was not attempted.

It should be plausible then to argue that the phenomenon observed in the present work was mainly due to the contribution of the spatial defects such as pores or micro-cracks on the hardness measurement and clearly not due to the alone ISE even if it can be present. Indeed, from a physical perspective, for instance at lower loads, e.g., 10 mN, the indentation volume was only ~0.25 μm^3 as opposed to ~1,450 μm^3 at 1,000 mN load on the plan section of the coating. Assuming a typical defect size of about 1 × 1 × 0.15 μm (Fig. 1), the number of defects encountered within the indentation volume at 10 mN load would be much smaller (~1) as opposed to about 10,000 at a load of 1,000 mN when a depth of about 3,500 nm was scanned (c.f., depth scanned at 10 mN load was ~170 nm). The role of such micro-structural defects (e.g., pores and cracks) was to reduce the total solid load bearing contact area. The lesser such reduction occurred inside the indentation volume; the relatively higher would be the measured magnitude of nano-hardness and Young's modulus, e.g., those evaluated at lower loads.

However, at higher loads, as a much larger depth was scanned, e.g., about 3,500 nm, the interaction scenario between the penetrating nanoindenter and the "characteristic microstructural flaws" of the present MIPS-HAP coating got inverted. The possibility of presence of such defects inside the indentation volume was enhanced, as explained above; thereby locally reducing significantly the total load bearing solid contact area of the coating [41, 42]. In correspondence, the coating registered a relatively lower magnitude of characteristic nano-hardness and Young's modulus when evaluated at higher loads (e.g., 1,000 mN) during the nanoindentation experiments. In conjunction, scanning electron microscopy had already showed that the deeper one goes from the very top surface toward the interior, the larger becomes the spatial density of the

"characteristic microstructural flaws" of the present MIPS-HAP coating [2].

Based on the present experimental evidences we therefore suggest that, independent and/or interdependent contributions from two important factors, e.g., (a) the enhancement in spatial density of flaws at higher depth and (b) the concomitant reduction in solid load bearing contact area inside the indentation volume might have added up to provide one of the possible genesis for ISE in nano-hardness and Young's moduli data as observed in the present work. In addition, it is also strongly suggested that in these conditions, it seems very difficult to separate the actual ISE from the defect influence in the indentation measurements and certainly deserves further detailed investigation into this genuine problem. Therefore, to summarize we may conclude that the present work demonstrates the presence of an "apparent indentation size effect" in the nano-hardness and Young's modulus data of the MIPS-HAP coating.

Another point should be mentioned in this connection. "Young's modulus" is measured in conventional macroscopic mechanical testing usually by tensile test using a tensile force on the specimen. In contrast, "bulk modulus" is measured from a volume deformation. It may be argued that since nanoindentation measurement causes a permanent deformation of the indented volume during the withdrawal of the penetrator, the corresponding modulus measured should be termed as a bulk modulus, rather than as a "Young's modulus". The interesting fact though is that the original work of Sneddon [43] considers the deformation of a semi infinite solid by a flat punch in terms of the reduced Young's modulus of the indenter-sample composite system. This was why following the seminal works of Doerner and Nix [44], Oliver and Pharr [20], Field and Swain [45], Mukhopadhyay and Paufler [23], etc., in this evolving field of "nanoindentation behavior of solid materials and coatings"; throughout the present work we have retained the term "Young's modulus".

The Weibull moduli, ("m") values of the nano-hardness data varied in the range 2–8 (Fig. 7a) for the plan section. Moreover, the "m" value increased systematically beyond 100 mN with the load to a value of, e.g., close to 8 at a higher load of 1,000 mN (Fig. 7a). Similar trend was exhibited by the "m" values of the Young's modulus data for the similar range of loads (Fig. 7b). Thus, there was an increasing trend of Weibull moduli values for both the nano-hardness and the Young's modulus data of the MIPS-HAP coating as the indentation load was enhanced from 10 to 1,000 mN. Here we propose an explanation for such observation.

The physical picture of the aforesaid phenomenon is schematically shown in Fig. 8 and it is proposed to be linked to the length scale of interaction phenomena between the penetrating nanoindenter and the "characteristic microstructural scale flaws and defects" of the MIPS-HAP coating. At relatively lower loads on the plan section (e.g., $p \leq 300$ mN), the nanoindent size almost scaled with the size of microstructural defects (Fig. 8: upper part) and being of the smaller size the nanoindent itself was most likely to have also negotiated many inter-splat boundaries, which were a typical weak, defect populated zone of the coating.

This situation possibly led to a high degree of interaction between the penetrating nanoindenter and the microstructural scale characteristic flaws and defects present in the vicinity of the indentation site. That high degree of

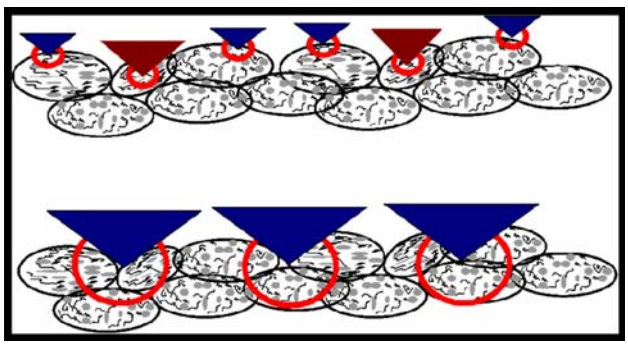

Fig. 8 Schematic of proposed qualitative model for indentation process at the plan section of MIPS-HAP coating: at low load (*upper part*) and at high load (*lower part*)

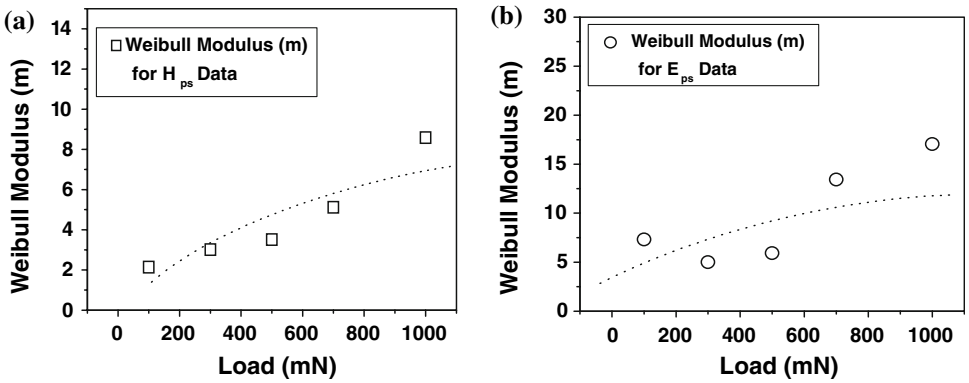

Fig. 7 Weibull modulus (m) values on plan section of MIPS-HAP coating as a function of load for **a** nano-hardness and **b** Young's moduli data

interaction caused a relatively higher degree of scatter in both nano-hardness and Young's modulus data and consequently a relatively lower "m" value, as observed in our experimental data also (Fig. 7a, b).

However, at relatively higher loads (e.g., 300 mN $< p \leq$ 1,000 mN) on the plan section, the nanoindent size was much bigger (Fig. 7a) than that obtained at relatively smaller loads (e.g., $p \leq$ 300 mN, Fig. 7b). Therefore, it covered a much larger number of splats and itself being much bigger in dimension, the nanoindent had the chance to negotiate with only a small number of inter-splat boundaries (Fig. 8: lower part).

As the number of inter-splat boundaries negotiated by the nanoindenter were ought to be smaller at relatively higher loads as mentioned above, relatively lesser were the chances of the interaction between the nanoindenter and the characteristic microstructural scale flaws and defects present at the weak inter-splat boundary. The lesser was the chance of interaction, the smaller was it's influence on the experimental data, thereby providing a scope for having a relatively lower scatter in the data as was indeed observed from the experimental data.

In addition, due to the relatively much larger indentation volume, e.g., $\sim$1,450 μm^3 created at higher load, i.e., 1,000 mN, the indentation cavity could encompass a much larger number of microstructural scale flaws and defects, all having most likely a very random spatial orientation. Thus, the interactions between the penetrating nanoindenter and the micro- as well as macro-structural defects, which had all very random spatial orientations in the present MIPS-HAP coatings, would be also having all possible types of spatial orientations in a random fashion. It is proposed that such randomly oriented interactions might have also cancelled out each others effect in such a way as to reduce the overall scatter in the data obtained at relatively higher loads (e.g., 300 mN $< p \leq$ 1,000 mN). If this picture were correct, there would be a general reduction expected in the scatter of both the nano-hardness and the Young's modulus data obtained at relatively higher loads of, e.g., (300 mN $< p \leq$ 1,000 mN). A reduction in data scatter should be reflected in relatively higher "m" values obtained at higher load nanoindentation experiments. The credence to such a picture was also borne out from the fact that the present experimental data showed an increasing trend of Weibull moduli with load (Fig. 7a, b) for both nano-hardness and Young's moduli data evaluated by the nanoindentation experiments with a Berkovich nanoindenter. Malzbender and Steinbrech [46] had also noted that for a sharp Vicker's indenter used for nanoindentation in plasma sprayed thermal barrier coating (TBC), the average uncertainty of measured hardness and Young's modulus decreased as the load was increased from 0.1 to 1 N.

Summary and conclusions

The major conclusions of the present work were:

(a) The nano-hardness and Young's modulus data were measured on polished plan section (PS) of the microplasma sprayed (MIPS) 230 μm thick highly porous, heterogeneous hydroxyapatite (HAP) coating on SS316L, by the nanoindentation technique with a Berkovich nanoindenter. The characteristic values of nano-hardness and Young's modulus were calculated through the application of Weibull statistics.

(b) Both the nano-hardness and Young's modulus data showed an "Apparent Indentation Size Effect (ISE)" as the load was varied from 10 to 1,000 mN. The apparent ISE was explained in terms of the variation in total load bearing solid contact area which was linked to different spatial scale and density of heterogeneous microstructural defects negotiated by the nanoindenter penetrating at lower and higher loads. In addition, it was also strongly suggested that in these conditions, it would be very difficult to separate the actual ISE from the defect influence in the indentation measurements and this genuine problem certainly deserves further, separate detailed investigation into it.

(c) There was an increasing trend of Weibull moduli values with load for both the nano-hardness and the Young's modulus data of the MIPS-HAP coating as the indentation load was enhanced from 10 to 1,000 mN. A qualitative model was suggested in the present work, to explain the load dependence of the Weibull moduli data.

Acknowledgements The authors are grateful to Director, Central Glass and Ceramic Research Institute (CGCRI), Kolkata for his kind permission to publish this paper and to Dr. D. K. Bhattacharya, Head, Analytical Facility Division of CGCRI for his kind encouragements during the course of this work. One of the authors (A.D.) also sincerely acknowledges the support and encouragements received from Prof. N. R. Bandyopadhyay of the School of Materials Science and Engineering, Bengal Engineering and Science University (BESU), Shibpur. The authors also appreciate the infrastructural support received from all colleagues and particularly those received from the colleagues of the Scanning Electron Microscopy Section, Mechanical Test Section, and Bio-Ceramics and Coating Division at CGCRI. Finally, the authors gratefully acknowledge financial support received from DST-SERC (Project No: GAP 0216) and CSIR (Network Project TAREMAC No: NWP 0027).

References

1. Dey A, Mukhopadhyay AK, Gangadharan S, Sinha MK, Basu D (2009) Mater Manuf Process 24(12)
2. Dey A, Mukhopadhyay AK, Gangadharan S, Sinha MK, Basu D, Bandyopadhyay NR (2009) Ceram Int 35:2295

3. Dey A, Mukhopadhyay AK, Gangadharan S, Sinha MK, Basu D (2008) In: Raghu Prasad BK, Narasimhan R (eds) Proceedings of interquadrennial conference of international congress on fracture, August 3–7, 2008, Bangalore, India. I. K. International Publishing House Pvt. Ltd., pp 311–313
4. Dey A, Mukhopadhyay AK, Gangadharan S, Sinha MK, Basu D (2008) In: Raghu Prasad BK, Narasimhan R (eds) Proceedings of interquadrennial conference of international congress on fracture, August 3–7, 2008, Bangalore, India. I. K. International Publishing House Pvt. Ltd., pp 217–219
5. Wen J, Leng Y, Chen J, Zhang C (2000) Biomaterials 21:1339
6. Zhang C, Leng Y, Chen J (2001) Biomaterials 22:1357
7. Khor KA, Li H, Cheang P (2003) Biomaterials 24:769
8. Cheng GJ, Pirzada D, Cai M, Mohanty P, Bandyopadhyay A (2005) Mater Sci Eng C 25:541
9. Chen Y, Zhang YQ, Zhang TH, Gan CH, Zheng CY, Yu G (2006) Carbon 44:37
10. Nieh TG, Jankowski AF, Koike J (2001) J Mater Res 16:3238
11. Nieh TG, Choi BW, Jankowski AF (2001) Minerals, Metals and Materials Society Annual Meeting and Exhibition
12. Arias JL, Mayor MB, Pou J, Leng Y, Leon B, Amora MP (2003) Biomaterials 24:3403
13. Gross KA, Samandari SS (2007) J Aus Ceram Soc 43:98
14. Zhang S, Wang YS, Zeng XT, Khor KA, Weng W, Sun DE (2008) Thin Solid Films 516:5162
15. Saber-Samandari S, Gross KA (2009) Surf Coat Tech (article in press). doi:10.1016/j.surfcoat.2009.05.033
16. Pelletier H, Nelea V, Mille P, Muller D (2004) J Mater Sci 39:3605. doi:10.1023/B:JMSC.0000030712.81704.b0
17. Zhou H, Li F, He B, Wang J, Sun B (2007) Surf Coat Tech 201:7360
18. Basu D, Funke C, Steinbrech RW (1999) J Mater Res 14:4643
19. Guo S, Kagawa Y (2006) Ceram Int 32:263
20. Oliver WC, Pharr GM (1992) J Mater Res 7:1564
21. Ma Q, Clarke DR (1995) J Mater Res 10:853
22. Bull SJ, Pag TF, Yoffe EH (1989) Phil Mag Lett 59:281
23. Mukhopadhyay NK, Paufler P (2006) Int Mater Rev 51:209
24. Mukhopadhyay NK, Bhatt J, Pramanik AK, Murty BS, Paufler P (2004) J Mater Sci 39:5155. doi:10.1023/B:JMSC.0000039202.27103.4c
25. Bernhardt EO (1941) Z Metallkd 33:135
26. Nix WD, Gao H (1998) J Mech Phys Solid 46:411
27. Horstemeyer MF, Baskes MI, Plimpton SJ (2001) Acta Mater 49:4363
28. Iost A, Bigot R (1996) J Mater Sci 31:3573. doi:10.1007/BF00360764
29. Li H, Gosh A, Han YH, Bradt RC (1993) J Mater Res 8:1028
30. Swain MV, Wittling M (1996) In: Bradt RC et al (eds) Fracture mechanics of ceramics, vol 11. Plenum Press, New York, p 379
31. Gong J, Guan Z (2001) Mater Lett 47:140
32. Gao YX, Fan H (2002) J Mater Sci 37:4493. doi:10.1023/A:1020662215932
33. Paternoster C, Fabrizi A, Cecchini R, Mehtedi ME, Choquet P (2008) J Mater Sci 43:3377. doi:10.1007/s10853-007-2392-1
34. Hays C, Kendall EG (1973) Metallography 6:275
35. Li H, Bradt RC (1991) Mater Sci Eng A 142:51
36. Peng Z, Gong J, Miao H (2004) J Eur Ceram Soc 24:2193
37. Taylor GI (1934) Proc R Soc London A 145:362
38. Taylor GI (1938) J Inst Metal 62:307
39. Kumar RR, Wang M (2002) Mater Sci Eng A 338:230
40. Huang Y, Zhang F, Hwang KC, Nix WD, Pharr GM, Feng G (2006) J Mech Phys Sol 54:1668
41. Mukhopadhyay AK, Phani KK (1998) J Mater Sci 33:69. doi:10.1023/A:1004385327370
42. Rossi RC (1968) J Am Ceram Soc 51:433
43. Sneddon IN (1965) Int J Eng Sci 3:47
44. Doerner MF, Nix WD (1986) J Mater Res 1:601
45. Field JS, Swain MV (1993) J Mater Res 8:297
46. Malzbender J, Steinbrech RW (2003) J Mat Res 18:1975